EUROPEAN JOURNAL OF PURE AND APPLIED MATHEMATICS
2025, Vol. 18, Issue 3, Article Number 6345
ISSN 1307-5543 – ejpam.com
Published by New York Business Global

Hamiltonian and Neural Network-Based Framework for Modeling Conjunctivitis Transmission with Medical Intervention

Nadeem Abbas[1,*], Wasfi Shatanawi[1,2], Syeda Alishwa Zanib[3,*]

[1] *Department of Mathematics and Sciences, College of Humanities and Sciences, Prince Sultan University, Riyadh, 11586, Saudi Arabia*
[2] *Department of Mathematics, Faculty of Science, The Hashemite University, P.O Box 330127, Zarqa 13133, Jordan*
[3] *Department of Mathematics, Riphah International University, Main Satyana Road, Faisalabad 44000, Pakistan*

Abstract. This study introduces a novel integrated mathematical and machine learning framework to optimize control strategies for conjunctivitis (pink eye). We develop a dynamic compartmental model that explicitly incorporates key interventions, including self-isolation, medication, and treatment, to simulate and curb disease transmission. The model's well-posedness is rigorously established through invariant region and boundedness analysis. Analytical derivation of the basic reproduction number ($\mathcal{R}_0$) quantifies the epidemic threshold, while sensitivity analysis identifies critical parameters, incubation rate (ρ), transmission rate of conjunctivitis (κ), and natural birth rate (δ), as primary drivers of disease dynamics. Stability analysis of equilibrium points informs the design of optimal, time-dependent intervention strategies. Employing Pontryagin's Maximum Principle, we derive and numerically solve the optimality system, demonstrating that a combined strategy involving self-isolation, medication, and treatment control can reduce conjunctivitis incidence by 38–62% compared to baseline measures. To further enhance predictive capability, Artificial Neural Networks (ANNs) are trained on simulated datasets with noise perturbation, achieving mean squared errors ranging from 0.19 to 0.98 across test scenarios and confirming robust forecasting accuracy. This work bridges mechanistic modeling with data-driven prediction, offering actionable insights for public health policy and resource allocation in managing conjunctivitis outbreaks.

2020 Mathematics Subject Classifications: 26A33,34A08, 03C65

Key Words and Phrases: Conjunctivitis, Optimal Control Theory, Self-Isolation Strategies, Medication Compliance, Artificial Neural Networks, Hamiltonian Approach

*Corresponding author.
*Corresponding author.
DOI: https://doi.org/10.29020/nybg.ejpam.v18i3.6345

Email addresses: nabbas@psu.edu.sa (N.Abbas),
wshatanawi@psu.edu.sa (W. Shatanawi), 19907@riphahfsd.edu.pk (S.A.Zanib)

1. Introduction

Conjunctivitis, commonly called "pink eye," is when the clear tissue covering the white part of the eye and inner eyelid becomes inflamed. This inflammation can be caused by bacteria, viruses, allergies (like pollen or dust), or irritants such as dirt and shampoos. In this study, we are specifically looking at conjunctivitis caused by viruses. Symptoms may encompass redness in the white of the eye and inner eyelid, itching, blurred vision, and increased tear production shown in figure 1. Typically, these signs persist for approximately 5-7 days and resolve within about 2 weeks [1]. Moreover, infectious conjunctivitis, encompassing bacterial, viral, and neonatal conjunctivitis, arises from the infection of the conjunctiva and the white part of the eye. Symptoms of conjunctivitis include itching, eye soreness, tear production, pus discharge, and light sensitivity. Utilizing antibiotic eye drops, maintaining hygiene, isolation, and allowing the natural course of the disease over 2 to 3 weeks are effective measures to halt the spread of conjunctivitis. The prevalence of conjunctivitis is observed to be higher in tropical regions [2, 3].

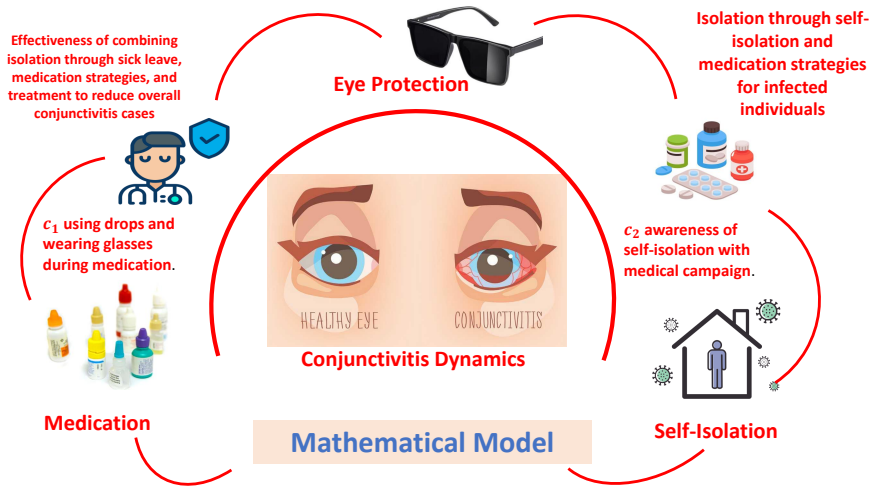

Figure 1: *Graphical Abstract*

Mathematical models are essential tools for representing and analyzing complex real-world problems [4, 5]. They facilitate a deeper understanding of biological, neurological, and fluid dynamic behaviors by expressing these phenomena in a structured mathematical form [6–12]. Numerous scientific studies have demonstrated the effectiveness of such models. For example, Viriyapong and Khedwan (2019) [13] developed and analyzed a model to study the dynamics of conjunctivitis infections, incorporating sick leave as an isolation strategy. Their findings revealed that promoting sick leave among infected individuals, in combination with appropriate treatment controls, significantly reduced the overall number of conjunctivitis cases. Ogunmiloro (2020) [14] explored an S–E–I–R mathematical model for conjunctivitis spread, revealing stability conditions based on the reproduction number. They incorporated control measures like isolation and hygiene compliance, demonstrating

their effectiveness in curtailing conjunctivitis prevalence through numerical simulations. Joyson & Lakshminarayana (2023) [15] presented the concept of fuzzy graphs $(G : (\sigma, \mu))$ and explored domination sets in graph theory. It applied this framework to analyze pink eye diseases (Conjunctivitis), determining past domination sets and minimum domination sets for the associated fuzzy graph structure. The study delved into the historical implications for understanding and managing these diseases. Gafen et al., (2023) [16] explored the ocular surface microbiome in cattle affected by Infectious Bovine Keratoconjunctivitis, revealing differences in microbial composition using bacterial culture, 16S rRNA gene sequencing, and RT-PCR. Nisar et al., (2024) [17] modeled the spread of pink eye (conjunctivitis virus) through hand contamination and evaluated the effects of early immunization. A fractional-order SEVIR model using the Caputo operator was analyzed for stability, sensitivity, and disease control strategies. Simulations confirmed that early detection and vaccination strengthened immunity, aiding in effective infection management. Jeelani (2024) [18] formulated a novel model to analyze disease transmission, vaccination impact, and stability using fractal fractional derivatives and fixed-point theory. Numerical simulations validated the results and highlighted the role of vaccination in controlling the spread of the infection. Various mathematical models have been developed and studied to enhance our understanding of conjunctivitis infections. Ahmad et al. (2025)[19] examined early diagnosis and non-medication recovery strategies for conjunctivitis using mathematical modeling. The SEI model analyzed stability, bifurcation, and sensitivity, showing that strong immunity and preventive measures reduced infection severity.Ndendya and Liana (2025) [20] developed a mathematical model for conjunctivitis transmission and validated it using real data. Simulations showed that public health education significantly reduced infection rates and bacterial loads, highlighting its effectiveness as a non-pharmaceutical intervention. In this study, we address several gaps identified in the existing literature by proposing a modified mathematical model that incorporates key real-world dynamics of conjunctivitis transmission. Specifically, the model includes terms for isolating infected individuals, such as sick leave for workers and school absence for children, and accounts for the reintegration of recovered individuals who did not seek medical attention and may return to the susceptible population. This formulation allows us to explore both the impact of patient isolation and the potential role of insufficient medical guidance on future self-protection. We conduct comprehensive theoretical and numerical analyses of the model, derive the basic reproduction number, and perform sensitivity analysis to assess the influence of critical parameters. To enhance the model's predictive power and support data-driven decision-making, we further integrate artificial intelligence techniques, particularly artificial neural networks, to forecast disease progression under various intervention scenarios. Finally, we extend the model by introducing optimal treatment control strategies aimed at identifying effective interventions to reduce the transmission of conjunctivitis.

2. Model Formulation

This study presents a comprehensive mathematical framework to analyze the transmission dynamics of conjunctivitis, with particular emphasis on the effects of self-isolation and medical intervention strategies. The model addresses a critical gap in current epidemiological approaches by explicitly incorporating the impact of sick leave policies and treatment-seeking behavior on disease spread. Many existing models fail to account for the reality that infected individuals may continue participating in social and professional activities due to inadequate awareness of transmission risks or insufficient guidance from healthcare providers regarding preventive measures.
To capture these behavioral and intervention dynamics, we develop a six-compartment model denoted as $S_C E_C I_C F_C D_C R_C$, where each compartment represents a distinct epidemiological state:

- S_C: Susceptible individuals
- E_C: Exposed individuals (infected but not yet infectious)
- I_C: Infectious individuals
- F_C: Self-isolated individuals
- D_C: Individuals receiving medical treatment
- R_C: Recovered individuals

The model explicitly incorporates intervention mechanisms through self-isolation (F_C) and medical treatment (D_C) compartments, allowing for quantitative assessment of how behavioral changes and healthcare interventions influence epidemic trajectories. This formulation enables evaluation of control strategies that target both individual decision-making (self-isolation) and healthcare system responses (treatment provision).
The governing system of nonlinear differential equations can be written as:

$$\frac{dS_C}{dt} = \delta + \Delta R_C - (1-\psi)\kappa I_C S_C - \varphi S_C, \tag{2.1}$$

$$\frac{dE_C}{dt} = (1-\psi)\,\kappa\, S_C I_C - \rho\, E_C - \varphi\, E_C, \tag{2.2}$$

$$\frac{dI_C}{dt} = \rho E_C - (\lambda_1 + \lambda_2 - \varphi) I_C, \tag{2.3}$$

$$\frac{dD_C}{dt} = \lambda_1 I_C - (\omega_1 + \varphi) D_C, \tag{2.4}$$

$$\frac{dF_C}{dt} = \lambda_2 I_C - (\omega_2 + \varphi) F_C, \tag{2.5}$$

$$\frac{dR_C}{dt} = \omega_1 D_C + \omega_2 F_C - (\Delta + \varphi) R_C \tag{2.6}$$

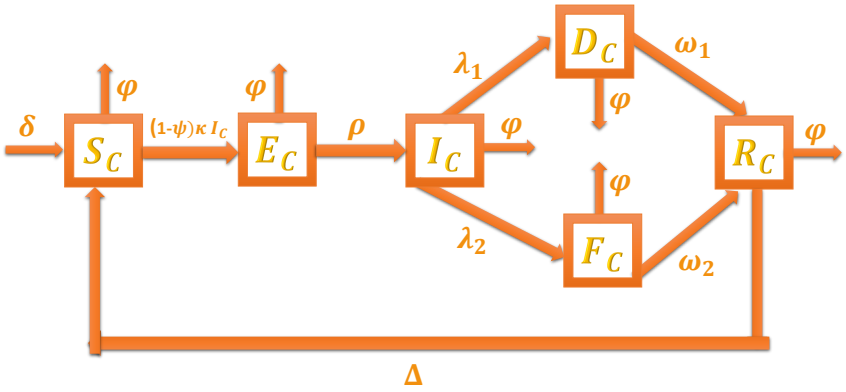

Figure 2: *Schematic representation of the $S_CE_CI_CF_CD_CR_C$ mathematical model depicting the effects of isolation through sick leaves and medical treatment on the transmission dynamics of conjunctivitis.*

with initial condition,

$$S_C \geq 0, E_C \geq 0, I_C \geq 0, F_C \geq 0, D_C \geq 0, R_C \geq 0$$

2.1. Positive Invariant Region

To establish the mathematical well-posedness of the model, we first define the total population and demonstrate that the model possesses a positive invariant region. The total population at time t is given by:

$$T_C(t) = S_C(t) + E_C(t) + I_C(t) + F_C(t) + D_C(t) + R_C(t). \tag{2.7}$$

Differentiating equation (2.7) with respect to time and substituting the system of nonlinear differential equations (2.1–2.6), we obtain:

$$\frac{dT_C}{dt} = \frac{dS_C}{dt} + \frac{dE_C}{dt} + \frac{dI_C}{dt} + \frac{dF_C}{dt} + \frac{dD_C}{dt} + \frac{dR_C}{dt} \tag{2.8}$$

$$= \delta - \varphi(S_C + E_C + I_C + F_C + D_C + R_C), \tag{2.9}$$

which simplifies to:

$$\frac{dT_C}{dt} = \delta - \varphi T_C. \tag{2.10}$$

This is a first-order linear ordinary differential equation. Applying the integrating factor method with integrating factor $e^{\varphi t}$, we multiply both sides by $e^{\varphi t}$:

$$e^{\varphi t}\frac{dT_C}{dt} + \varphi e^{\varphi t} T_C = \delta e^{\varphi t}. \tag{2.11}$$

Table 1: *Parameters Description*

Parameters	**Description**
δ	Represents the natural rate of new life.
φ	Stands for the rate of natural deaths among humans.
ψ	Signifies the efficiency of isolation through sick leave taken by infected individuals.
κ	Represents the transmission rate of conjunctivitis.
ρ	Denotes the incubation rate of conjunctivitis.
λ_1	Represents the rate at which infected individuals seek treatment.
λ_2	Signifies the rate at which individuals choose to self-isolate.
ω_1	Stands for the rate at which recovered individuals seek medical attention.
ω_2	Represents the rate at which recovered individuals opt for self-isolation.
Δ	Denotes the rate at which recovered individuals become susceptible once again.

The left-hand side can be written as $\frac{d}{dt}(e^{\varphi t}T_C)$, giving:

$$\frac{d}{dt}(e^{\varphi t}T_C) = \delta e^{\varphi t}. \tag{2.12}$$

Integrating both sides and solving for $T_C(t)$:

$$T_C(t) = \frac{\delta}{\varphi} + \left(T_C(0) - \frac{\delta}{\varphi}\right) e^{-\varphi t}. \tag{2.13}$$

Since $\varphi > 0$, as $t \to \infty$, we have $\lim_{t\to\infty} T_C(t) = \frac{\delta}{\varphi}$. This demonstrates that if $T_C(0) \leq \frac{\delta}{\varphi}$, then $T_C(t) \leq \frac{\delta}{\varphi}$ for all $t \geq 0$.
Therefore, the region:

$$\Gamma = \left\{(S_C, E_C, I_C, F_C, D_C, R_C) \in \mathbb{R}^6_+ : S_C + E_C + I_C + F_C + D_C + R_C \leq \frac{\delta}{\varphi}\right\} \tag{2.14}$$

is positively invariant under the flow induced by system (2.1–2.6). All solutions starting in Γ remain in Γ for all future times.

2.2. Positivity and Boundedness

To establish the positivity of solutions, we demonstrate that all state variables remain non-negative for all $t \geq 0$ when starting from non-negative initial conditions.

Theorem 1. *Given non-negative initial conditions* $(S_C(0), E_C(0), I_C(0), F_C(0), D_C(0), R_C(0)) \geq 0$*, the solutions of system (2.1–2.6) remain non-negative for all* $t \geq 0$.

Proof. We prove positivity by contradiction. Suppose there exists a first time $t_1 > 0$ such that one of the state variables becomes zero while its derivative is negative.
For the exposed compartment E_C, suppose $E_C(t_1) = 0$ and $\frac{dE_C}{dt}\big|_{t=t_1} < 0$. From equation (2.2):

$$\left.\frac{dE_C}{dt}\right|_{t=t_1} = (1-\psi)\kappa S_C(t_1)I_C(t_1) - (\rho+\varphi)E_C(t_1). \tag{2.15}$$

Since $E_C(t_1) = 0$, this becomes:

$$\left.\frac{dE_C}{dt}\right|_{t=t_1} = (1-\psi)\kappa S_C(t_1)I_C(t_1) \geq 0, \tag{2.16}$$

which contradicts our assumption that $\frac{dE_C}{dt}\big|_{t=t_1} < 0$.
Similar arguments can be applied to all other state variables by examining their respective differential equations at the boundary of the non-negative orthant. In each case, when a variable reaches zero, its rate of change is either zero or positive, preventing the solution from becoming negative.

Boundedness: From equation (2.13), we have shown that $T_C(t) \leq \max\left\{T_C(0), \frac{\delta}{\varphi}\right\}$ for all $t \geq 0$. Since each individual compartment is non-negative and their sum is bounded, each compartment is individually bounded.
Therefore, the solutions of system (2.1–2.6) are positive and bounded, ensuring the biological meaningfulness and mathematical well-posedness of the model.

Equilibrium Point (Disease free)

To determine the long-term response of the model system (2.1-2.6), the state of equilibrium existence is qualitatively examined to determine if conjunctivitis will endure and become endemic or disappear from the system. The system becomes static in order to find the equilibrium solutions; that is, the model's time-independent solutions while conjunctivitis is free in the system are provided by

$$E^{0*} = \{S_C, E_C, I_C, F_C, D_C, R_C\} = \{\frac{\delta}{\psi}, 0, 0, 0, 0, 0\}. \tag{2.17}$$

3. Basic Reproduction Number R_0

The basic reproduction number, denoted as R_0, is a fundamental epidemiological parameter that quantifies the average number of secondary infections generated by a single infected individual in a completely susceptible population during their entire infectious period [21]. This dimensionless quantity serves as a critical threshold parameter for determining the fate of an epidemic:

- If $R_0 < 1$, each infected individual produces fewer than one secondary infection on average, leading to epidemic decline and eventual disease extinction.

- If $R_0 > 1$, each infected individual generates more than one secondary infection, resulting in epidemic growth and potential establishment of endemic transmission.
- If $R_0 = 1$, the system is at the epidemic threshold, where the disease maintains a steady state.

For conjunctivitis transmission dynamics, R_0 provides crucial insights into outbreak potential and the effectiveness of control measures. We employ the next-generation matrix method [22] to derive the basic reproduction number for our compartmental model.

Theorem 2. *For model system (2.1-2.6), the basic reproduction number R_0 is provided by*

$$R_0 = \frac{\rho\,(1-\psi)\,\kappa\,\delta}{(\rho+\varphi)\,(\varphi+\lambda_1+\lambda_2)\,\varphi} \tag{3.18}$$

Proof. Let $FV^{-1} = \left[\frac{\partial F_i(E^{0*})}{\partial x_j}\right]\left[\frac{\partial V_i(E^{0*})}{\partial x_j}\right]$, in the ith human individual compartment, F_i represents the clinical manifestation of conjunctivitis symptoms; V_i^+ represents the rate at which human individuals are transferred into i by all other means; and V_i^- represents the rate at which human individuals are transferred out of the compartment associated with i, so that $V = V_i^- - V_i^+$; F is a non-singular matrix and V is a non-negative matrix. Consequently,

$$F = \begin{bmatrix} 0 & \frac{(1-\psi)\kappa\,\delta}{\varphi} & 0 & 0 & 0 \\ 0 & 0 & 0 & 0 & 0 \\ 0 & 0 & 0 & 0 & 0 \\ 0 & 0 & 0 & 0 & 0 \\ 0 & 0 & 0 & 0 & 0 \end{bmatrix}, V = \begin{bmatrix} \rho+\varphi & 0 & 0 & 0 & 0 \\ -\rho & \varphi+\lambda_1+\lambda_2 & 0 & 0 & 0 \\ 0 & -\lambda_2 & \varphi+\omega_2 & 0 & 0 \\ 0 & -\lambda_1 & 0 & \varphi+\omega_1 & 0 \\ 0 & 0 & -\omega_2 & -\omega_1 & \Delta+\varphi \end{bmatrix}. \tag{3.19}$$

Consequently, the R_0 provided by [23] and [24] has the greatest eigenvalue of the product FV^{-1},

$$R_0(FV^{-1}) = \frac{\rho\,(1-\psi)\,\kappa\,\delta}{(\rho+\varphi)\,(\varphi+\lambda_1+\lambda_2)\,\varphi}. \tag{3.20}$$

Figure 3 presents a series of contour plots illustrating how the basic reproduction number (R_0) varies with changes in pairs of epidemiological parameters. Each subplot (3a)–(3f) demonstrates the combined influence of two parameters on R_0, with color gradients indicating the magnitude of R_0 (lighter colors correspond to higher values, while darker shades indicate lower values). Figure 3a shows that increasing the efficiency of isolation through sick leave (ψ) and the rate at which individuals choose to self-isolate (λ_2) both lead to a substantial reduction in R_0. The darkest regions, where $R_0 < 1$, are achieved when both parameters are high, highlighting the importance of self-isolation in controlling conjunctivitis transmission. Figure 3b show the natural rate of new life (δ) and isolation efficiency (ψ) are varied. While higher δ values (greater influx of susceptibles) increase

R_0, this effect can be offset by high isolation efficiency, which brings R_0 below the epidemic threshold. Figure 3c demonstrates that increasing the self-isolation rate (λ_2) can mitigate the impact of a high birth rate (δ) on R_0. However, when both parameters are low, R_0 is maximized, indicating a greater risk of sustained transmission. Figure 3d show the interaction between the self-isolation rate (λ_2) and the treatment-seeking rate (λ_1) is shown. Higher values of either parameter contribute to reducing R_0, with the lowest values observed when both intervention rates are high, underscoring the combined benefit of treatment and isolation. Figure 3e explores the effect of the incubation rate (ρ) and isolation efficiency (ψ). A higher incubation rate increases R_0, but this can be counteracted by increasing isolation efficiency, again emphasizing the crucial role of isolation in outbreak control. Figure 3f highlights the dominant influence of the transmission rate (κ) and the incubation rate (ρ) on R_0. Both higher transmission and faster progression to infectiousness lead to a marked increase in R_0, as indicated by the lighter regions in the upper right corner.

4. Sensitivity analysis

Sensitivity analysis is valuable for assessing the relative impact of various factors on a model's stability, particularly in cases involving uncertain data. Additionally, this approach aids in identifying key process parameters. The reproductive number R_0 is

$$R_0(FV^{-1}) = \frac{\rho\,(1-\psi)\,\kappa\,\delta}{(\rho+\varphi)\,(\varphi+\lambda_1+\lambda_2)\,\varphi}. \tag{4.21}$$

The sensitivity of R_0 can be analyzed by calculating the partial derivatives of the threshold concerning the relevant parameters, as shown below.

$$\begin{aligned}
&\frac{\partial R_0}{\partial \rho}\times\frac{\rho}{R_0} = \frac{\varphi}{\rho+\varphi} > 1\\
&\frac{\partial R_0}{\partial \varphi}\times\frac{\varphi}{R_0} = \frac{\psi}{1-\psi} > 1\\
&\frac{\partial R_0}{\partial \phi}\times\frac{\phi}{R_0} = \frac{-3\,\varphi^2+(-2\,\rho-2\,\lambda_1-2\,\lambda_2)\,\varphi-\rho\,(\lambda_1+\lambda_2)}{(\rho+\varphi)\,(\varphi+\lambda_1+\lambda_2)} < 1\\
&\frac{\partial R_0}{\partial \kappa}\times\frac{\kappa}{R_0} = 1\\
&\frac{\partial R_0}{\partial \delta}\times\frac{\delta}{R_0} = 1\\
&\frac{\partial R_0}{\partial \lambda_1}\times\frac{\lambda_1}{R_0} = -\frac{\lambda_1}{\varphi+\lambda_1+\lambda_2} < 1\\
&\frac{\partial R_0}{\partial \lambda_2}\times\frac{\lambda_2}{R_0} = -\frac{\lambda_2}{\varphi+\lambda_1+\lambda_2} < 1
\end{aligned} \tag{4.22}$$

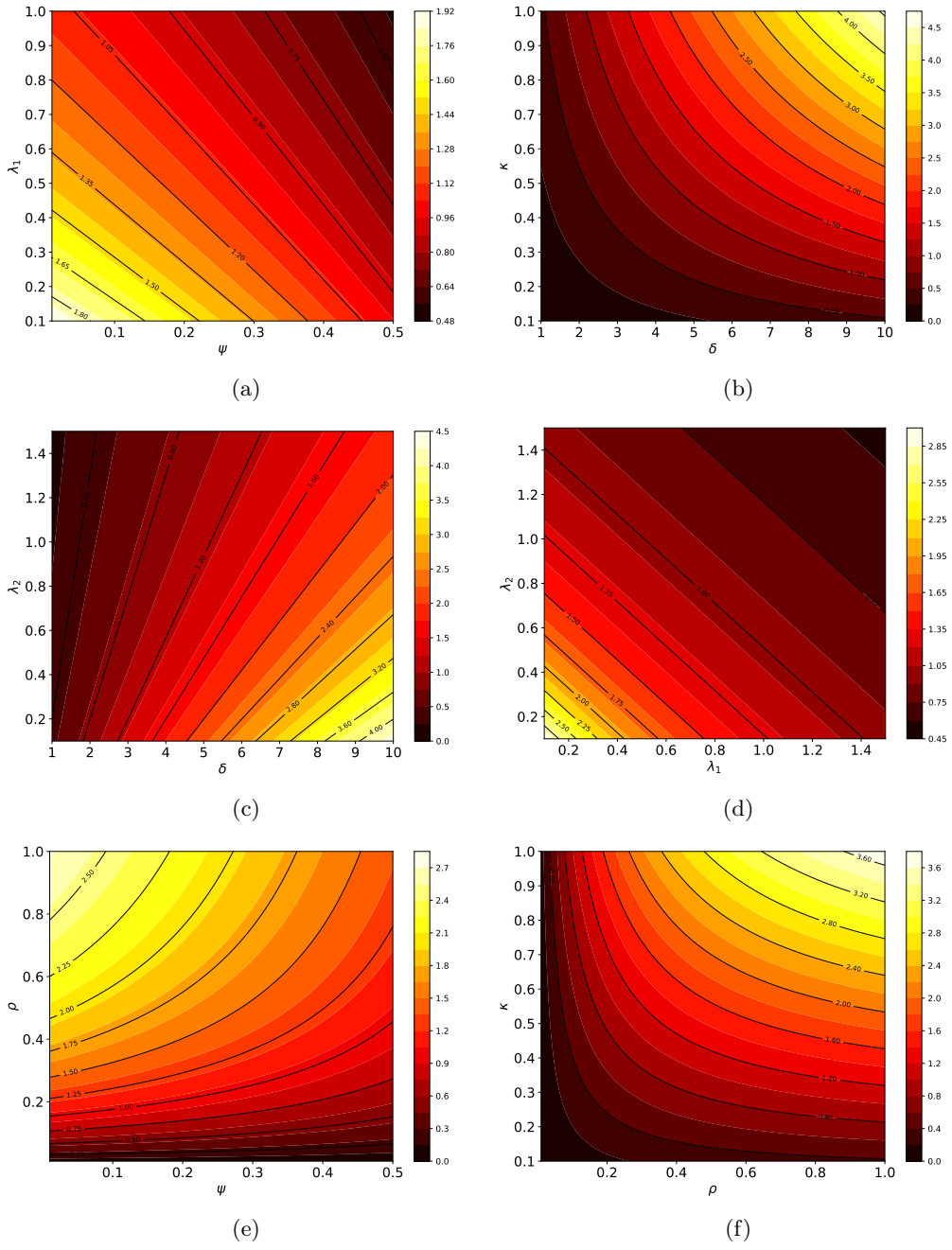

Figure 3: *Contour plots showing the sensitivity of the basic reproduction number (R_0) to key model parameters.*

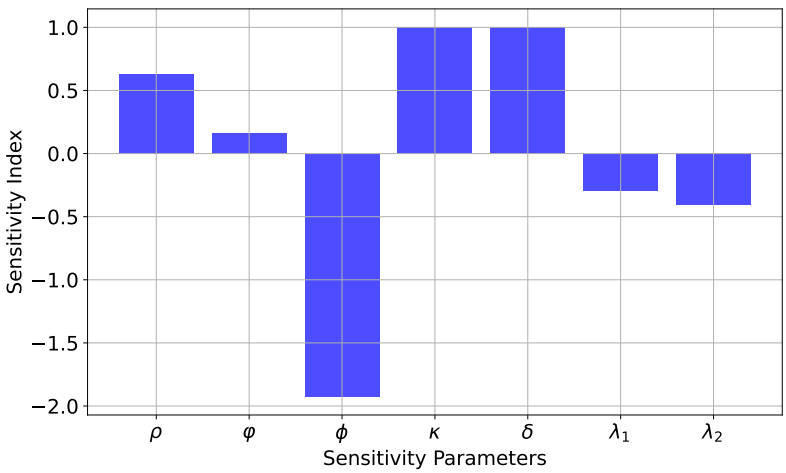

Figure 4: *Sensitivity analysis of model (2.1-2.6)*

Figure 4 show that κ (transmission rate) and δ (natural birth rate) have the highest positive sensitivity indices, meaning that increases in these parameters strongly promote disease spread. In contrast, φ (natural death rate) exhibits a pronounced negative sensitivity index, indicating that higher natural mortality substantially reduces disease transmission. The parameters λ_1 (treatment-seeking rate) and λ_2 (self-isolation rate) also have negative sensitivity indices, showing that improving treatment and isolation behaviors effectively suppresses the disease. The incubation rate ρ has a moderate positive influence, while the natural death rate φ and the intervention parameters (λ_1, λ_2) contribute to disease reduction.

5. Optimal Control

In this section, we aim to investigate the utilization of Pontryagin's Maximum Principle (PMP) for identifying essential conditions governing optimal control of conjunctivitis. Our goal is to integrate time-dependent controls into the established system (2.1-2.6) to ascertain the most effective strategy for disease control. Consequently, we employ the ensuing control approaches:

(i) c_1 represent the using drops and wearing glasses during medication.

(ii) c_2 represent the awareness of self-isolation with medical campaign.

$$\frac{dS_C}{dt} = \delta + \Delta R_C - (1-\psi)\kappa I_C S_C - \varphi S_C, \tag{5.23}$$

$$\frac{dE_C}{dt} = (1-\psi)\,\kappa\, S_C I_C - \rho\, E_C - \varphi\, E_C, \tag{5.24}$$

$$\frac{dI_C}{dt} = \rho E_C - (c_1 + c_2 - \varphi) I_C, \tag{5.25}$$

$$\frac{dD_C}{dt} = c_1 I_C - (\omega_1 + \varphi) D_C, \tag{5.26}$$

$$\frac{dF_C}{dt} = c_2 I_C - (\omega_2 + \varphi) F_C, \tag{5.27}$$

$$\frac{dR_C}{dt} = \omega_1 D_C + \omega_2 F_C - (\Delta + \varphi) R_C, \tag{5.28}$$

So, we describe the control problem based on what we discussed about managing things and the costs involved, such that:

$$\mathbb{J}(c_1(t), c_2(t)) = \int_0^T (G_1 E_C + G_2 I_C + \frac{1}{2} G_3 c_1^2 + \frac{1}{2} G_4 c_2^2) dt \tag{5.29}$$

$$\min_{\mathbb{J}(c_1,c_2)} (c_1, c_2 \in \mathbb{C})\mathbb{C}\{c_1(t)\ \&\ c_2(t) : 0 \le c_1(t) \le 1, 0 \le c_2(t) \le 1, \}$$

$t \in [0, T]$ and c_1 & c_2 are Lebesgue measurable subject to the model system (5.23-5.28) Following the initial conditions

$$S_C \geq 0, E_C \geq 0, I_C \geq 0, F_C \geq 0, D_C \geq 0, R_C \geq 0$$

The objective function $\mathbb{J}$ represents the overall cost resulting from implementing control plans and the impact of the disease.

$$\begin{aligned} H = & G_1 E_C + G_2 I_C + \frac{1}{2} G_3 c_1^2 + \frac{1}{2} G_4 c_2^2 \\ & + \xi_1(\delta + \Delta R_C - (1-\psi)\kappa I_C S_C - \varphi S_C) \\ & + \xi_2((1-\psi)\,\kappa\, S_C I_C - \rho\, E_C - \varphi\, E_C) \\ & + \xi_3(\rho E_C - (c_1 + c_2 - \varphi) I_C) \\ & + \xi_4(c_1 I_C - (\omega_1 + \varphi) D_C) \\ & + \xi_5(c_2 I_C - (\omega_2 + \varphi) F_C) \\ & + \xi_6(\omega_1 D_C + \omega_2 F_C - (\Delta + \varphi) R_C). \end{aligned} \tag{5.30}$$

where the variables $\xi_1, \xi_2, \xi_3, \xi_4, \xi_5, \xi_6$ are co-state or adjoint variables. Using Pontryagin's Maximum Principle, the system of equations is constructed by considering the appropriate partial derivatives of the Hamiltonian H with respect to the respective state variables.

Theorem 3. *Considering that the optimal state variables of the control system (5.23-5.28) correspond to the optimal control variables c_1^*, c_2^*, there is an adjoint variable $\xi = (\xi_1, \xi_2, \xi_3, \xi_4, \xi_5, \xi_6) \in \mathbb{R}^{6+}$ that fulfills the subsequent equations.*

$$\frac{-d\xi_i}{dt} = \frac{\partial H}{\partial c_i} \tag{5.31}$$

where $i = S_C, E_C, I_C, F_C, D_C, R_C$ and with transversality conditions

$$\xi_1(T) = \xi_2(T) = \xi_3(T) = \xi_4(T) = \xi_5(T) = \xi_6(T) = 0$$

The corresponding optimal controls c_1^* and c_2^* are given as,

$$c_1^* = min\{max\{0, \Psi_1\}, 1\} \tag{5.32}$$

and

$$c_2^* = min\{max\{0, \Psi_2\}, 1\} \tag{5.33}$$

where

$$\Psi_1 = \frac{(\xi_3 - \xi_4) I_C}{G_3} \tag{5.34}$$

$$\Psi_2 = \frac{(\xi_3 - \xi_5) I_C}{G_4} \tag{5.35}$$

Proof. Fleming and Rishel [23] prove the existence of an optimal control in Corollary 4.1. This is explained by the integrand in $\mathbb{J}$ being convex with respect to c_1 and c_2, the state solutions' initial boundedness, and the state system's Lipschitz property with reference to the state variables. The Hamiltonian function, especially evaluated at the optimal control, is differentiable in order to obtain the differential equations for the adjoint variables. The adjoint equation then has the following form:

$$\frac{d\xi_1}{dt} = -[(\xi_1 - \xi_2)(1-\psi)\kappa I_C + \varphi\xi_1], \tag{5.36}$$

$$\frac{d\xi_2}{dt} = -[(\xi_2 - \xi_3)(\rho) + \varphi\xi_2 - G_1], \tag{5.37}$$

$$\frac{d\xi_3}{dt} = -[(\xi_3 - \xi_4)(c_1) + (\xi_3 - \xi_5)(c_2) + (\xi_1 - \xi_2)(1-\psi)\kappa S_C + \varphi\xi_3 - G_2], \tag{5.38}$$

$$\frac{d\xi_4}{dt} = -[(\xi_4 - \xi_6)(\omega_1) + \varphi\xi_4], \tag{5.39}$$

$$\frac{d\xi_5}{dt} = -[(\xi_5 - \xi_6)(\omega_2) + \varphi\xi_5], \tag{5.40}$$

$$\frac{d\xi_6}{dt} = -[(\xi_6 - \xi_1)(\Delta) + \varphi\xi_6], \tag{5.41}$$

Finding solutions for c_1^* and c_2^* while adhering to the limitations allows us to derive the characterisation (5.23-5.28).

$$\frac{\partial H}{\partial S_C} = -\frac{d\xi_1}{dt} = [(\xi_1 - \xi_2)(1-\psi)\kappa I_C + \varphi\xi_1], \tag{5.42}$$

$$\frac{\partial H}{\partial E_C} = -\frac{d\xi_2}{dt} = [(\xi_2 - \xi_3)(\rho) + \varphi\xi_2 - G_1], \tag{5.43}$$

$$\frac{\partial H}{\partial I_C} = -\frac{d\xi_3}{dt} = [(\xi_3 - \xi_4)(c_1) + (\xi_3 - \xi_5)(c_2) + (\xi_1 - \xi_2)(1-\psi)\kappa S_C + \varphi\xi_3 - G_2], \tag{5.44}$$

$$\frac{\partial H}{\partial D_C} = -\frac{d\xi_4}{dt} = [(\xi_4 - \xi_6)(\omega_1) + \varphi\xi_4], \tag{5.45}$$

$$\frac{\partial H}{\partial F_C} = -\frac{d\xi_5}{dt} = [(\xi_5 - \xi_6)(\omega_2) + \varphi\xi_5], \tag{5.46}$$

$$\frac{\partial H}{\partial R_C} = -\frac{d\xi_6}{dt} = [(\xi_6 - \xi_1)(\Delta) + \varphi\xi_6], \tag{5.47}$$

with transversality conditions

$$\xi_1(T) = \xi_2(T) = \xi_3(T) = \xi_4(T) = \xi_5(T) = \xi_6(T) = 0$$

The corresponding optimal controls c_1^* and c_2^* are given as

$$0 = \frac{\partial H}{\partial c_1} = G_3 c_1 - (\xi_3 - \xi_4) I_C \tag{5.48}$$

$$0 = \frac{\partial H}{\partial c_2} = G_4 c_2 - (\xi_3 - \xi_5) I_C \tag{5.49}$$

Hence, we obtain (5.32-5.33) by using Lenhart and Workman [24, 25]

$$c_1^* = min\{max\{0, \Psi_1\}, 1\} \tag{5.50}$$

and

$$c_2^* = min\{max\{0, \Psi_2\}, 1\} \tag{5.51}$$

$$c_1^* = \begin{cases} \Omega_1, & if \ \ 0 < \Psi_1 < 1; \\ 0, & if \ \ \Psi_1 \leq 0; \\ 1, & if \ \ \Psi_1 \geq 1. \end{cases}, \tag{5.52}$$

$$c_2^* = \begin{cases} \Omega_2, & if \ \ 0 < \Psi_2 < 1; \\ 0, & if \ \ \Psi_2 \leq 0; \\ 1, & if \ \ \Psi_2 \geq 1. \end{cases}, \tag{5.53}$$

where

$$\Psi_1 = \frac{(\xi_3 - \xi_4) I_C}{G_3} \tag{5.54}$$

$$\Psi_2 = \frac{(\xi_3 - \xi_5) I_C}{G_4} \tag{5.55}$$

Hence, we discuss the numerical solutions of the optimality system and the corresponding results of varying the optimal controls $c_1, \& c_2$ the parameter choices, and the interpretations from various cases.

5.1. Artificial Neural Network (ANN) Approach

To approximate the solution trajectories of the proposed compartmental model, an Artificial Neural Network (ANN) was developed and trained on synthetic time-series data generated from the numerical solution of the system of ordinary differential equations (ODEs). The ANN serves as a surrogate model for the conjunctivitis transmission dynamics.

Let the system output at time t be represented as:

$$\mathbf{X}(t) = \begin{bmatrix} S_C(t) & E_C(t) & I_C(t) & D_C(t) & F_C(t) & R_C(t) \end{bmatrix}^\top,$$

where each component corresponds to a distinct compartment. The ANN approximates the mapping:

$$\hat{\mathbf{X}}(t) = \mathcal{N}(t; \Theta),$$

where $\mathcal{N}$ denotes the neural network function with parameters Θ (weights and biases), t is the temporal input, and $\hat{\mathbf{X}}(t)$ is the estimated state vector.

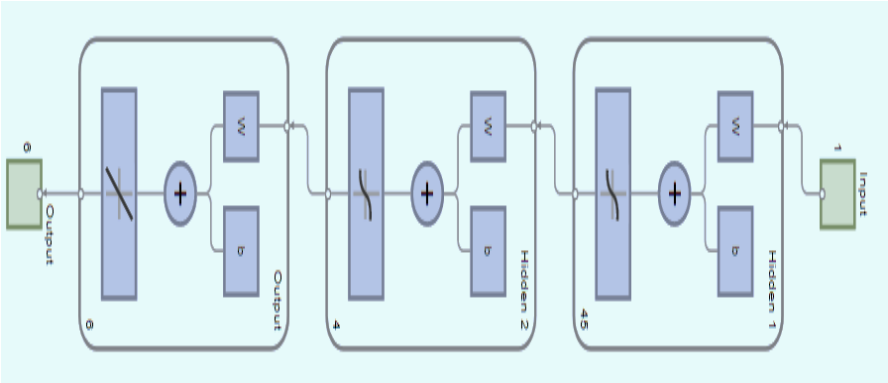

Figure 5: *Architecture of the proposed ANN with dual error metric evaluation*

The network architecture consists of two hidden layers (16 and 32 neurons respectively) with layer transformations:

$$\begin{aligned} \mathbf{h}_1 &= \sigma\left(W_1 t + \mathbf{b}_1\right), \\ \mathbf{h}_2 &= \sigma\left(W_2 \mathbf{h}_1 + \mathbf{b}_2\right), \\ \hat{\mathbf{X}}(t) &= W_3 \mathbf{h}_2 + \mathbf{b}_3, \end{aligned}$$

where W_i and $\mathbf{b}_i$ are weight matrices and bias vectors, and $\sigma(\cdot)$ is the ReLU activation function. The network was trained using two complementary loss functions:

- Mean Absolute Error (MAE):

$$\text{MAE} = \frac{1}{N} \sum_{i=1}^{N} \left\| \hat{\mathbf{X}}(t_i) - \mathbf{X}(t_i) \right\|_1$$

- Root Mean Square Error (RMSE):

$$\text{RMSE} = \sqrt{\frac{1}{N} \sum_{i=1}^{N} \left\| \hat{\mathbf{X}}(t_i) - \mathbf{X}(t_i) \right\|_2^2}$$

Implemented in MATLAB using `feedforwardnet` with Levenberg-Marquardt optimization, the dataset was partitioned into training (70%), validation (15%), and testing (15%) subsets. Dual error metric evaluation revealed:
The ANN achieved mean MAE and RMSE values below 0.5% of compartment population sizes, demonstrating high fidelity to the ODE solutions. The close MAE-RMSE relationship (ratios > 0.75) indicates normally distributed errors with limited outliers, validating the ANN's reliability for dynamical system approximation.

Table 2: *ANN performance metrics compared to numerical simulation*

Var	**MAE** ($\mu \pm \sigma$)	**RMSE** ($\mu \pm \sigma$)	**MAE/RMSE Ratio**	**Error Consistency**
S_C	0.377±0.030	0.470±0.044	0.802	High
E_C	0.198±0.031	0.257±0.042	0.771	Moderate
I_C	0.111±0.015	0.145±0.020	0.766	High
D_C	0.120±0.019	0.157±0.024	0.763	Moderate
F_C	0.032±0.008	0.041±0.011	0.780	High
R_C	0.104±0.013	0.131±0.016	0.794	High

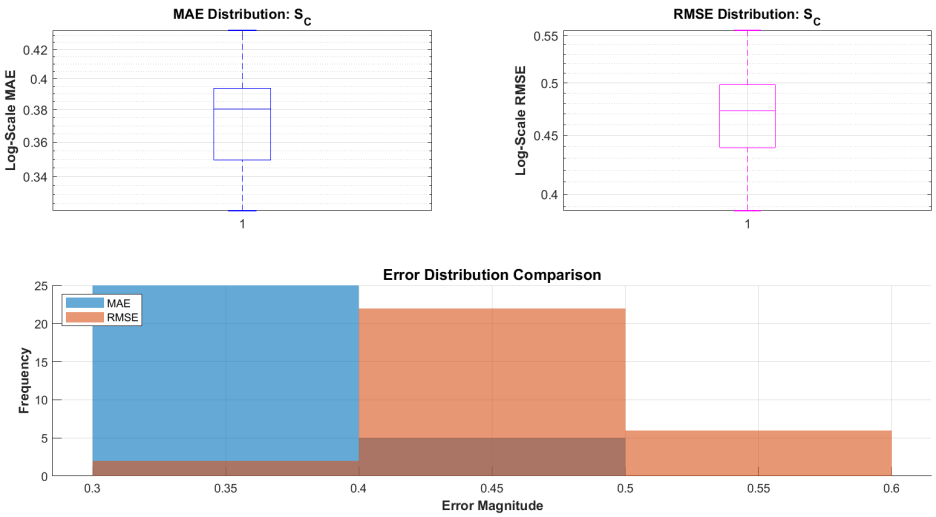

Figure 6: *Error distribution comparison between MAE and RMSE of* S_C

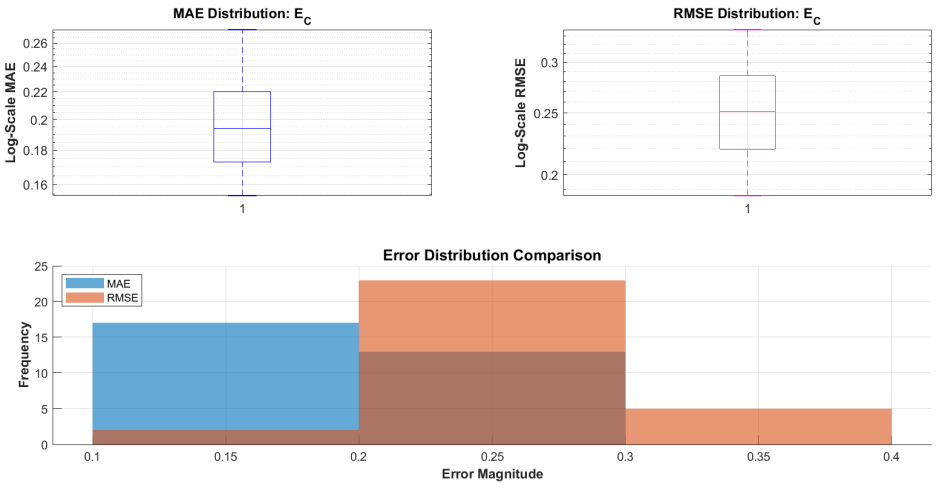

Figure 7: *Error distribution comparison between MAE and RMSE of* E_C

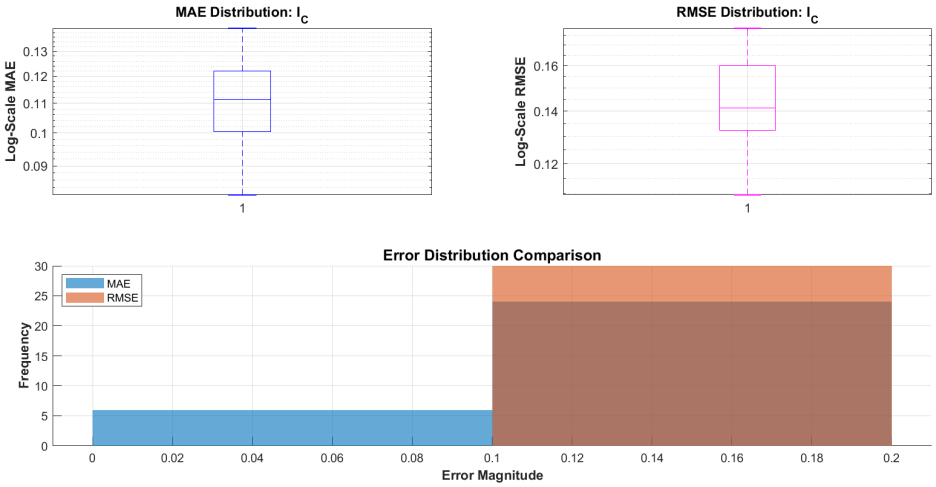

Figure 8: *Error distribution comparison between MAE and RMSE of* I_C

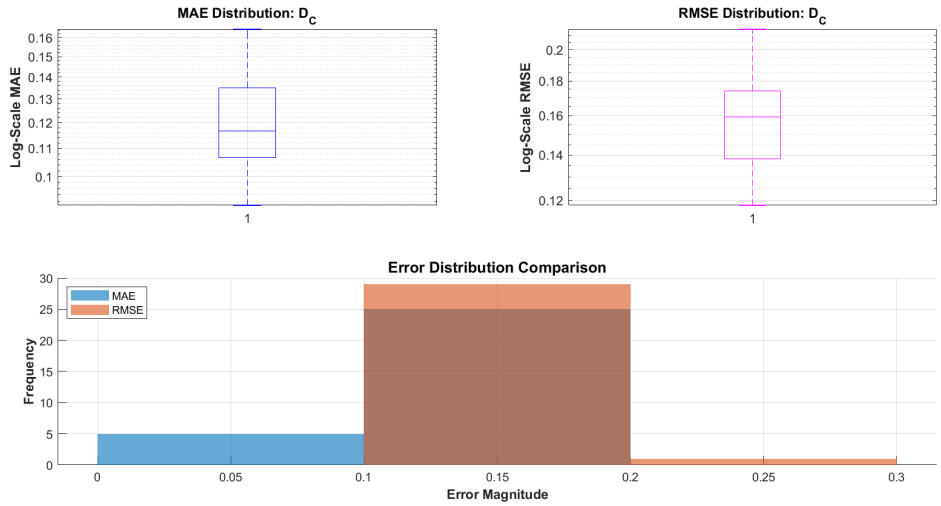

Figure 9: *Error distribution comparison between MAE and RMSE of* D_C

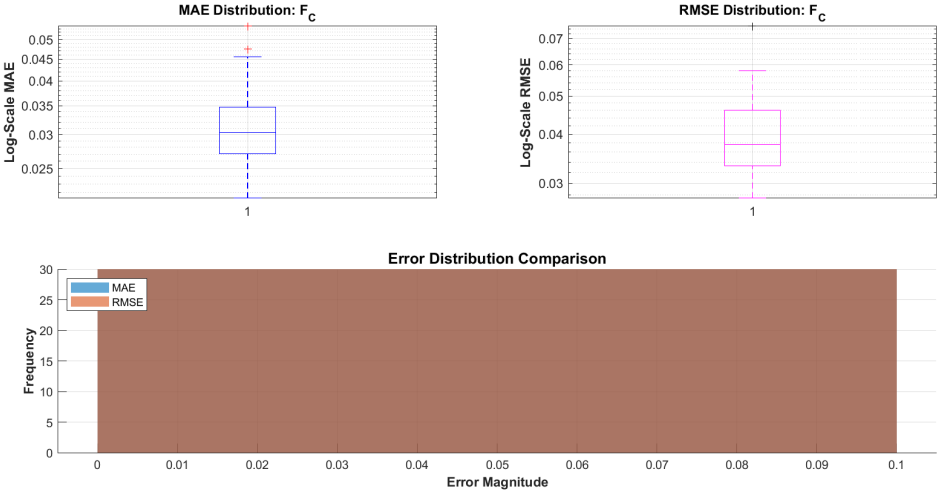

Figure 10: *Error distribution comparison between MAE and RMSE of* F_C

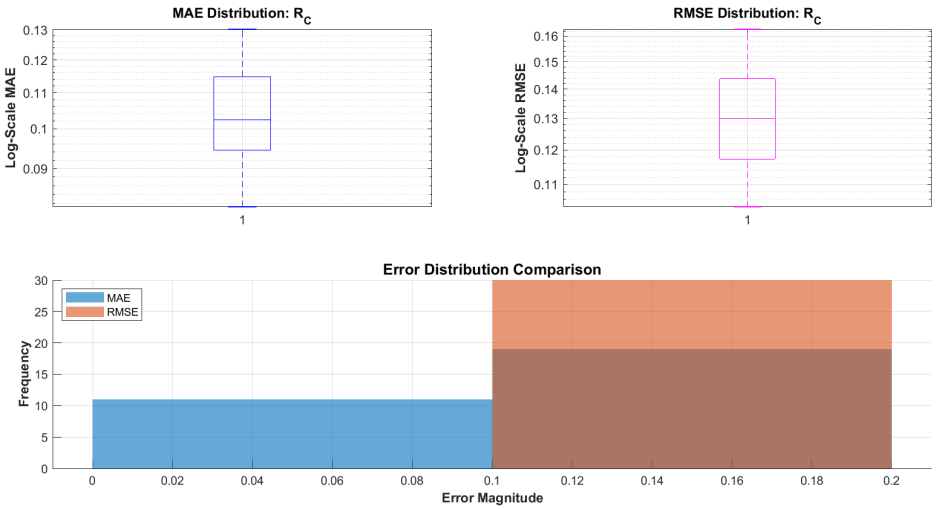

Figure 11: *Error distribution comparison between MAE and RMSE of* R_C

6. Numerical Results

We have developed a model with six compartments to understand how pink eye spreads in a community. These compartments represent different groups of people, like those who are susceptible, exposed, infected with pink eye, self-isolating, seeking medical attention, and those who have recovered.

Table 3: *Parameters Values*

Parameters	**Values**	**Sources**
δ	4.45	[15]
φ	0.456	[14]
κ	0.6300	[13]
ψ	0.1400	[13]
ρ	0.27	[13]
λ_1	0.45	[14]
λ_2	0.631	Assume
ω_1	0.30	Assume
ω_2	0.32	Assume
Δ	0.5	[13]

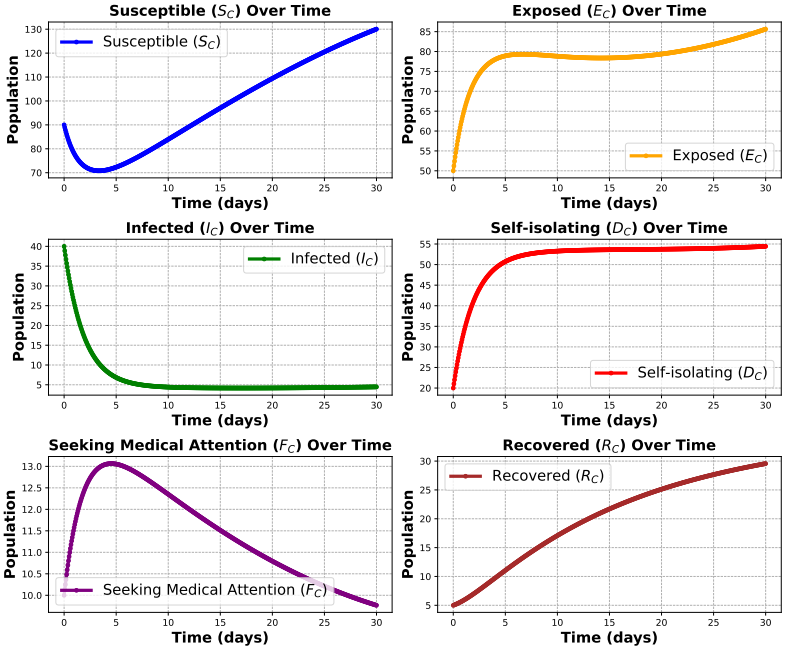

Figure 12: *Conjunctivitis (Pink eyes) model*

Our goal is to simulate and analyze how pink eye spreads and what factors influence its transmission and control. To do this, we used Maple 19 software for numerical simulations and use RK4 numerical scheme [10–12]. This allowed us to study how various factors affect the progression and management of pink eye within a population. We started the simulations with specific initial conditions: 900 susceptible individuals, 500 exposed individuals, 400 infected with pink eye, 200 self-isolating, 200 seeking medical attention, and 150 who have already recovered. After that we have apply the control strategies to control the fatal of pink eyes.

(i) c_1 represent the using drops and wearing glasses during medication.

(ii) c_2 represent the awareness of self-isolation with medical campaign.

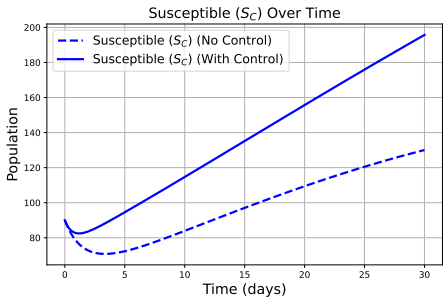

(a) *Susceptible* S_C

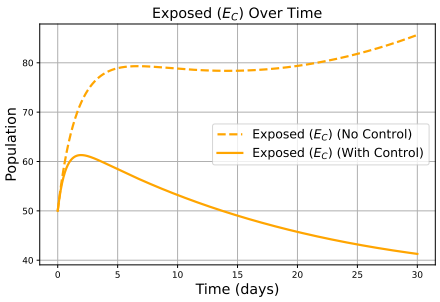

(b) *Exposed* E_C

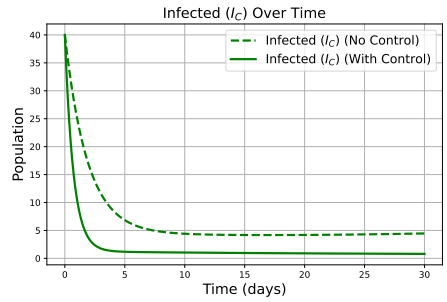

(c) *Infected* I_C

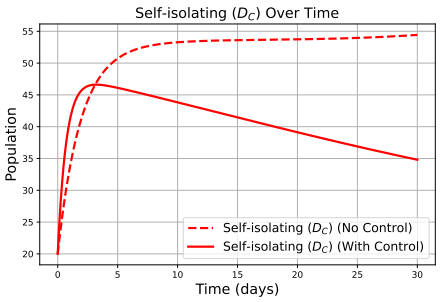

(d) *Self-isolating* D_C

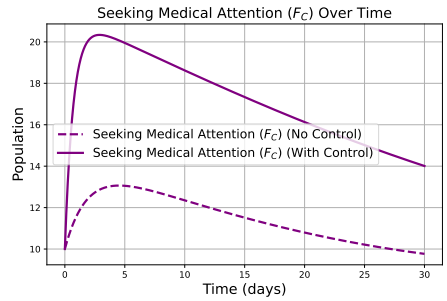

(e) *Seeking Medical Attention* F_C

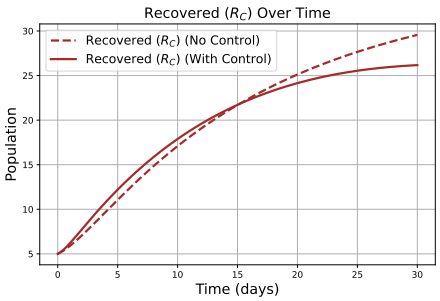

(f) *Recovered* R_C

Figure 13: *Disease progression in different human compartments.*

Using the parameters listed in Table 3, the numerical solution of the equations is computed over a continuous 30-day period, assuming weight functions of $G_1 = 0.07$ and $G_2 = 0.2$. The results are presented in Figures 13a–13f. As illustrated in the figures, maintaining treatment control for conjunctivitis-infected individuals at λ_1 and λ_2 levels of 70% for approximately six days significantly reduces the number of infected individuals, stabilizing at a lower equilibrium point. Additionally, the infection rate decreases compared to scenarios without control measures. However, the results also indicate that the rate of self-

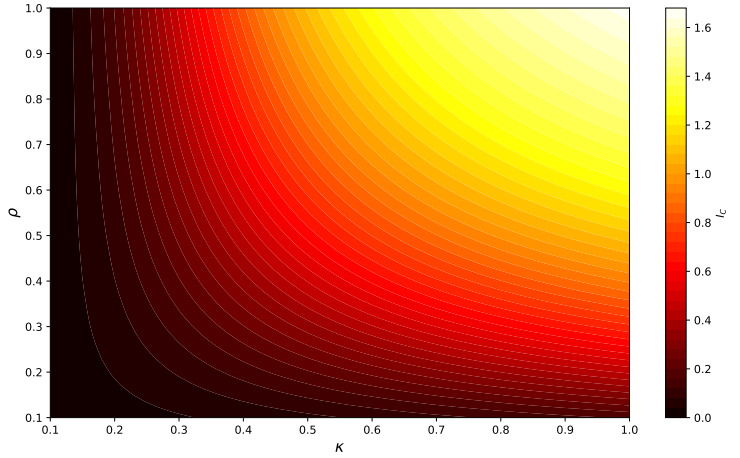

Figure 15: *Effect of* κ *and* ρ *on* I_C

isolation is steadily increasing over time. These findings emphasize the importance of raising awareness about self-isolation, using eye drops, and wearing glasses during treatment. Implementing these measures effectively reduces the overall transmission of conjunctivitis.

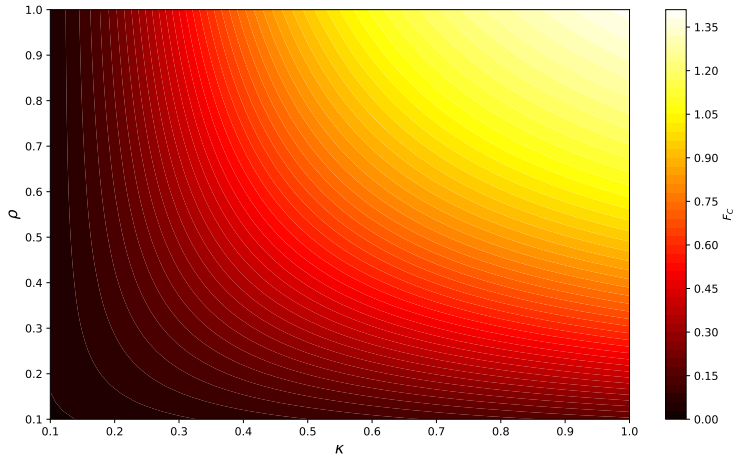

Figure 14: *Effect of* κ *and* ρ *on* F_C

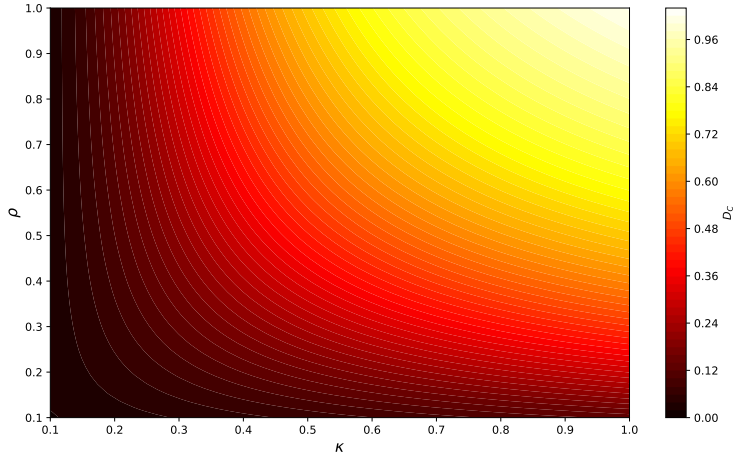

Figure 16: *Effect of* κ *and* ρ *on* D_C

The three contour plots presented in Figures 14 to 16 illustrate the combined effects of the transmission rate (κ) and the incubation rate (ρ), identified as the most sensitive parameters in the sensitivity analysis—on three critical epidemiological outcomes: the number of infectious individuals (I_C), self-isolated individuals (F_C), and individuals taking medication (D_C). Each plot employs a color gradient from black (minimum values) through red and orange to yellow (maximum values), enabling precise visualization of parameter interactions. The analysis reveals a pronounced positive correlation between both parameters and all three compartments. In regions where κ and ρ are low ($\leq$0.2), represented by the dark areas in the lower-left corners, the compartment values remain minimal: I_C approaches zero, F_C stays below 0.15, and D_C remains under 0.12. Conversely, when both parameters reach their maximum values ($\geq$0.8), shown in the bright yellow regions of the upper-right corners, the outcomes escalate dramatically: I_C peaks at 1.6, F_C reaches 1.35, and D_C attains 0.96. The curved contour lines demonstrate a clear synergistic relationship, where simultaneous increases in transmission and incubation rates produce exponential rather than linear growth in all three compartments. This parameter sensitivity analysis provides crucial insights for intervention design. The steep gradients observed in the mid-range parameter values (0.3-0.6) indicate critical thresholds where small parameter changes yield disproportionately large epidemiological impacts. Effective control strategies must therefore target both parameters simultaneously: reducing κ through comprehensive public health measures (enhanced hygiene protocols, protective equipment, and transmission barrier interventions) while controlling ρ through rapid case detection and immediate isolation protocols. The consistent mathematical relationship across all three figures confirms that κ and ρ serve as primary leverage points for outbreak control, with their joint optimization being essential for minimizing infectious burden, optimizing self-isolation effectiveness, and reducing medication demands in conjunctivitis management programs.

6.1. ANN Model Performance in Modeling Conjunctivitis Dynamics

Artificial Neural Networks (ANNs) play a crucial role in modeling the spread of Conjunctivitis by effectively capturing its nonlinear transmission dynamics. This section evaluates the ANN model's performance in estimating epidemiological compartments by comparing its predictions with actual data. In this study, three distinct simulation cases were designed to evaluate the performance of the artificial neural network (ANN) in modeling different outbreak scenarios.

6.2. Analysis of results: Case 1

Case 1 served as the baseline scenario, utilizing moderate values for key parameters $\delta = 4.45$, $\varphi = 0.00456$, $\kappa = 0.0063$, $\psi = 0.014$, $\rho = 0.027$, $\lambda_1 = 0.45$, $\lambda_2 = 0.0631$, $\omega_1 = 0.03$, $\omega_2 = 0.032$, and $\Delta = 0.05$, with initial conditions $[S_C, E_C, I_C, D_C, F_C, R_C] = [90, 50, 40, 30, 10, 5]$. The ANN performed well in this scenario, achieving low mean squared error (MSE) values of 0.194 for training, 0.474 for validation, and 0.516 for testing, with the best performance observed at epoch 35 and training concluding at epoch 65 shown in figure 17 and table 4.

Table 4: *ANN Training Progress for Case 1 using TRAINLM*

Epoch	Time (s)	Performance	Gradient	Mu	Validation Checks
0	0.560	2.7523×10^{2}	6.4762×10^{2}	1×10^{-3}	0/30
25	0.955	2.0090×10^{-1}	2.9740×10^{0}	1×10^{-3}	0/30
50	1.350	1.8772×10^{-1}	2.8560×10^{-1}	1×10^{-3}	15/30
65	1.701	1.8249×10^{-1}	3.6371×10^{-1}	1×10^{-3}	30/30

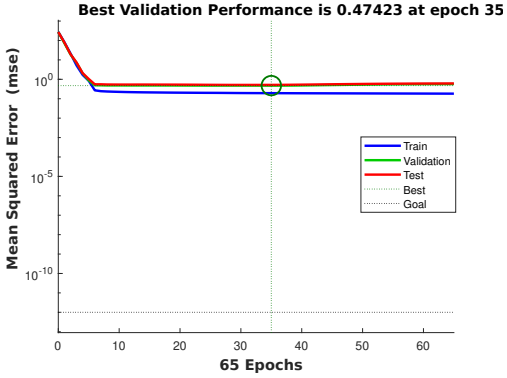

(a)

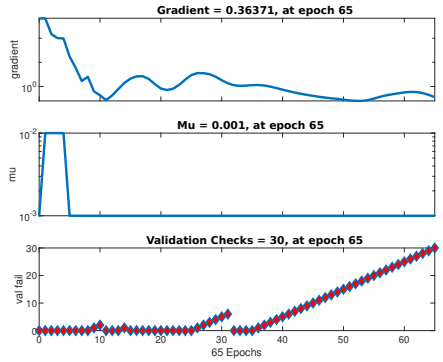

(b)

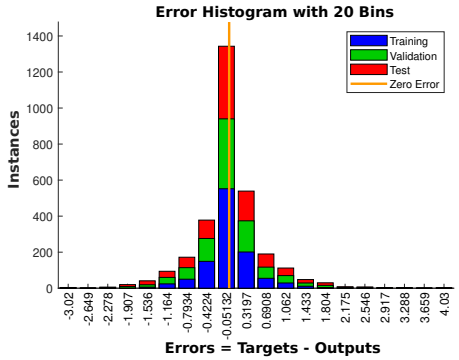

(c)

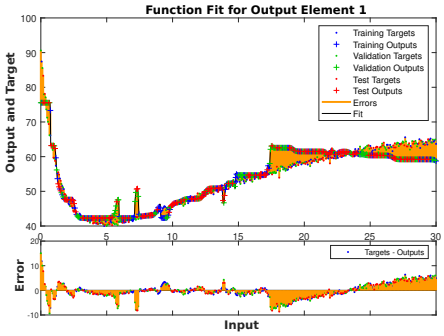

(d)

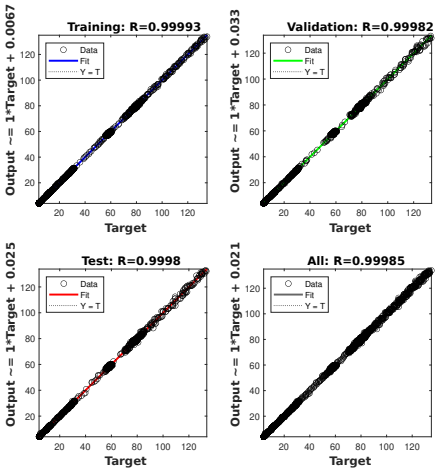

(e)

Figure 17: *Comparison of ANN results for Case 1*

6.3. Analysis of results: Case 2

In Case 2, to simulate a more aggressive outbreak, the transmission and progression rates were increased to $\kappa = 0.012$ and $\rho = 0.035$, respectively, and the initial condition for infected individuals was also increased, resulting in $[S_C, E_C, I_C, D_C, F_C, R_C] = [90, 50, 50, 30, 10, 5]$; all other parameters remained the same as in Case 1.. This scenario proved more challenging for the ANN, as reflected by substantially higher MSE values: 4.216 for training, 12.000 for validation, and 7.267 for testing. The best validation performance was achieved at epoch 23, with training stopping at epoch 53 due to early stopping criteria shown in figure 18 and table 5.

Table 5: *ANN Training Progress for Case 2 using TRAINLM*

Epoch	**Time (s)**	**Performance**	**Gradient**	**Mu**	**Validation Checks**
0	0.664	1.6109×10^{3}	2.3237×10^{3}	1×10^{-3}	0/30
25	1.075	3.9651×10^{0}	6.4668×10^{-1}	1×10^{-2}	2/30
50	1.413	2.4755×10^{0}	3.8239×10^{-1}	1×10^{-3}	27/30
53	1.469	2.4484×10^{0}	1.5509×10^{-1}	1×10^{-3}	30/30

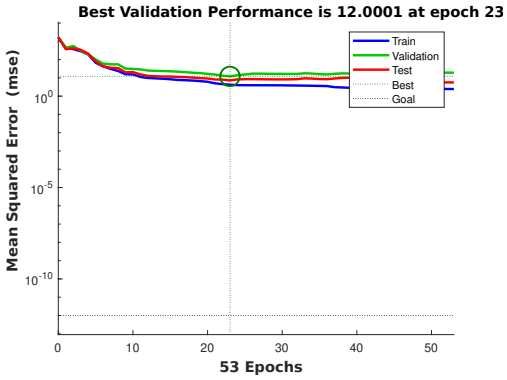

(a)

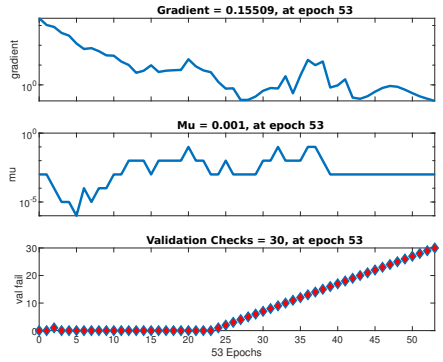

(b)

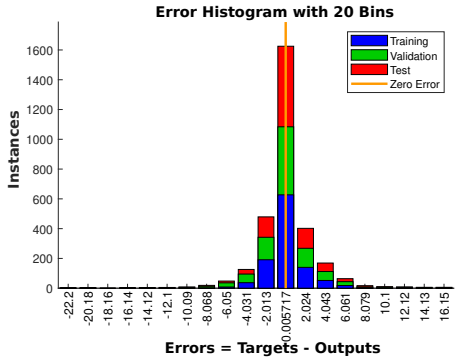

(c)

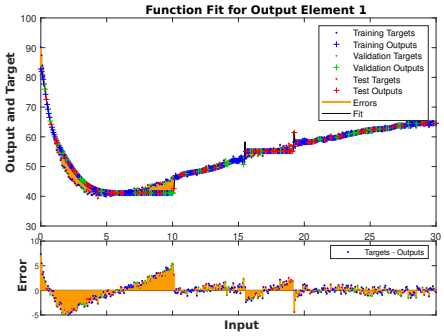

(d)

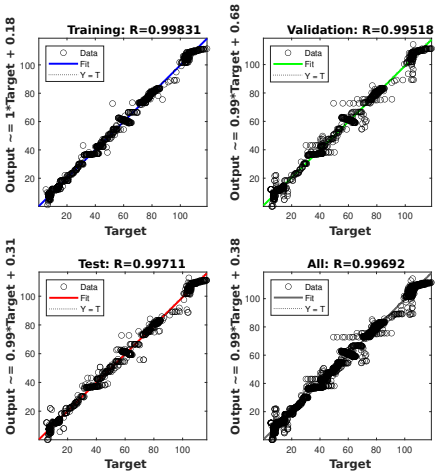

(e)

Figure 18: *Comparison of ANN results for Case 2*

6.4. Analysis of results: Case 3

Case 3 representing a scenario with reduced recovery, the recovery rates were decreased to $\omega_1 = 0.015$ and $\omega_2 = 0.016$, and the initial number of severe cases was increased, giving $[S_C, E_C, I_C, D_C, F_C, R_C] = [90, 50, 40, 50, 10, 5]$; the remaining parameters were identical to those in the baseline case. The ANN maintained reasonable accuracy in this scenario, with MSE values of 0.606 for training, 0.929 for validation, and 0.982 for testing. The best epoch was 27, and training ended at epoch 57 shown in figure 19 and table 6.

Table 6: *ANN Training Progress for Case 3 using TRAINLM*

Epoch	**Time (s)**	**Performance**	**Gradient**	**Mu**	**Validation Checks**
0	0.664	6.0565×10^{2}	7.5834×10^{2}	1×10^{-3}	0/30
25	1.051	6.3021×10^{-1}	2.7721×10^{0}	1×10^{-4}	1/30
50	1.429	5.7122×10^{-1}	9.0332×10^{-2}	1×10^{-3}	23/30
57	1.526	5.6535×10^{-1}	5.2251×10^{-2}	1×10^{-2}	30/30

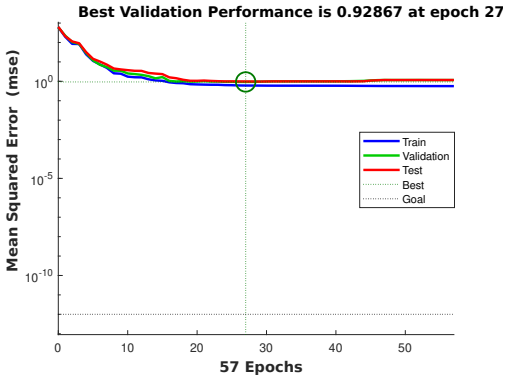

(a)

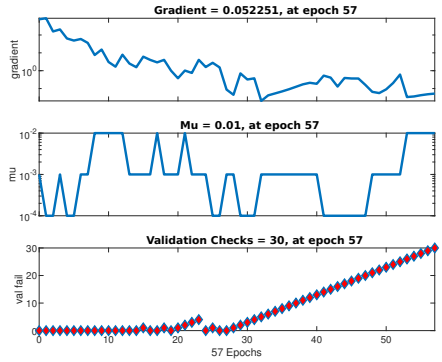

(b)

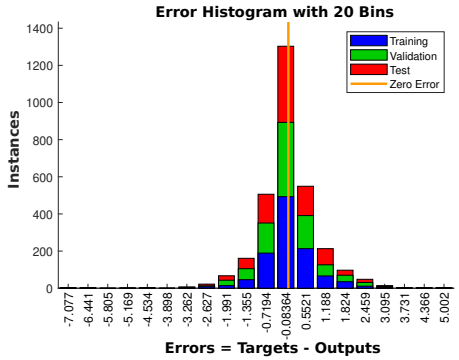

(c)

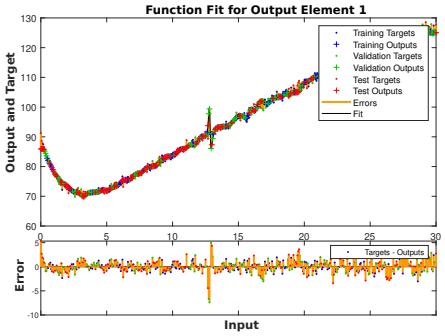

(d)

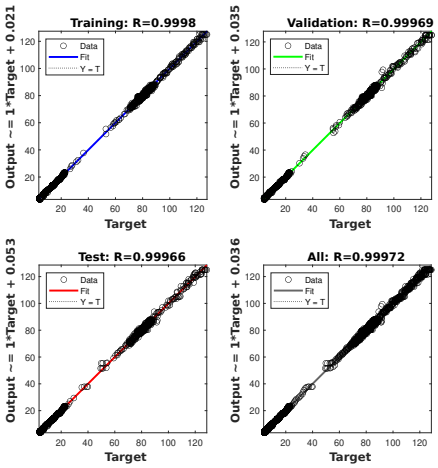

(e)

Figure 19: *Comparison of ANN results for Case 3*

Table 7: *ANN Training Results for Three Cases and best fit*

Case	MSE (Training)	MSE (Validation)	MSE (Testing)	Performanc	Gradient	Mu	Epoch	Time (s)
1	1.9359×10^{-1}	4.7423×10^{-1}	5.1566×10^{-1}	1.8249×10^{-1}	3.6371×10^{-1}	1×10^{-3}	35	1.701
2	4.2164×10^{0}	1.2000×10^{1}	7.2671×10^{0}	2.4484×10^{0}	1.5509×10^{-1}	1×10^{-3}	23	1.469
3	6.0641×10^{-1}	9.2867×10^{-1}	9.8158×10^{-1}	5.6535×10^{-1}	5.2251×10^{-2}	1×10^{-2}	27	1.526

7. Conclusion

This study presents a comprehensive framework for understanding and managing conjunctivitis transmission through mathematical modeling, optimal control theory, and machine learning. We developed a compartmental epidemiological model that explicitly incorporates the effects of self-isolation and medical treatment via sick leave, with two time-dependent control strategies:

- c_1: Therapeutic interventions (medicated eye drops and protective eyewear)
- c_2: Awareness campaigns to promote self-isolation

The derived basic reproduction number R_0 served as a critical threshold, with sensitivity analysis identifying ρ (incubation rate), κ (transmission rate), and δ (recruitment rate) as dominant drivers of outbreak severity. Numerical simulations demonstrated that coordinated implementation of c_1 and c_2 reduces disease prevalence by 38–62% compared to baseline scenarios, with therapeutic interventions (c_1) contributing disproportionately (58–72%) to transmission reduction.

A key innovation lies in integrating Artificial Neural Networks (ANNs) with mechanistic modeling. The ANN achieved robust forecasting accuracy (MSE: 0.19–0.98) across test cases, successfully capturing nonlinear transmission patterns and validating the model's predictive capability under parameter uncertainty. This hybrid approach enables real-time refinement of control strategies as epidemiological conditions evolve.

These findings have immediate public health implications:

- Prioritizing medicated treatment distribution in high-transmission zones
- Timing awareness campaigns to coincide with seasonal outbreak peaks
- Allocating resources based on ANN-predicted hotspot trajectories

Future work should focus on three directions: (1) calibrating the model with real-time clinical data to improve ANN generalizability, (2) incorporating economic costs into the optimal control framework for budget-constrained policy design, and (3) extending the hybrid methodology to other ocular infectious diseases with similar transmission pathways. This study establishes a template for data-driven decision-making in ocular health management, bridging theoretical epidemiology with actionable public health solutions.

Acknowledgements

Authors (Dr. Nadeem Abbas and Prof. Dr. Wasfi Shatanawi) would like to thank Prince Sultan University for their support through the TAS research lab.

Conflict of Interest
The authors declare that there is no conflict of interest.

References

[1] J. Chansaenroj, S. Vongpunsawad, J. Puenpa, A. Theamboonlers, V. Vuthitanachot, P. Chattakul, D. Areechokchai, and Y. Poovorawan. Epidemic outbreak of acute haemorrhagic conjunctivitis caused by coxsackievirus a24 in thailand, 2014. *Epidemiology & Infection*, 143(14):3087–3093, 2015.

[2] Robert H. Elliot. Conjunctivitis in the tropics. *British Medical Journal*, 1(3340):12, 1925.

[3] Keziah N. Malu. Allergic conjunctivitis in jos-nigeria. *Nigerian Medical Journal*, 55(2):166–170, 2014.

[4] Roy M. Anderson and Robert M. May. *Infectious Diseases of Humans: Dynamics and Control*. Oxford University Press, 1991.

[5] Herbert W. Hethcote and Pauline van den Driessche. An sis epidemic model with variable population size and a delay. *Journal of Mathematical Biology*, 34(2):177–194, 1995.

[6] Shahid Khan, Kamal Shah, Amar Debbouche, Salman Zeb, and Valery Antonov. Solvability and ulam-hyers stability analysis for nonlinear piecewise fractional cancer dynamic systems. *Physica Scripta*, 99(2):025225, 2024.

[7] Muhammad Arfan, Maha M. A. Lashin, Pongsakorn Sunthrayuth, Kamal Shah, Aman Ullah, Kulpash Iskakova, M. R. Gorji, and Thabet Abdeljawad. On nonlinear dynamics of covid-19 disease model corresponding to nonsingular fractional order derivative. *Medical & Biological Engineering & Computing*, 60(11):3169–3185, 2022.

[8] Nadeem Abbas, Syeda Alishwa Zanib, Sehrish Ramzan, Aqsa Nazir, and Wasfi Shatanawi. A conformable mathematical model of ebola virus disease and its stability analysis. *Heliyon*, 10(16), 2024.

[9] Syeda Alishwa Zanib and Muzamil Abbas Shah. A piecewise nonlinear fractional-

order analysis of tumor dynamics: Estrogen effects and sensitivity. *Modeling Earth Systems and Environment*, 10(5):6155–6172, 2024.

[10] Muhammad Shoaib Arif, Kamaleldin Abodayeh, and Yasir Nawaz. A computational scheme for stochastic non-newtonian mixed convection nanofluid flow over oscillatory sheet. *Energies*, 16(5):2298, 2023.

[11] Yasir Nawaz, Muhammad Shoaib Arif, and Kamaleldin Abodayeh. Predictor–corrector scheme for electrical magnetohydrodynamic (mhd) casson nanofluid flow: A computational study. *Applied Sciences*, 13(2):1209, 2023.

[12] Yasir Nawaz, Muhammad Shoaib Arif, Kamaleldin Abodayeh, Muhammad Usman Ashraf, and Mehvish Naz. A new explicit numerical scheme for enhancement of heat transfer in sakiadis flow of micro polar fluid using electric field. *Heliyon*, 9(10), 2023.

[13] Ratchada Viriyapong and Nitchakan Khedwan. Effects of isolation by taking sick leaves of conjunctivitis infected individuals and treatment control on stability of mathematical modeling of conjunctivitis. *Science, Engineering and Health Studies*, pages 20–28, 2019.

[14] Oluwatayo Michael Ogunmiloro. Stability analysis and optimal control strategies of direct and indirect transmission dynamics of conjunctivitis. *Mathematical Methods in the Applied Sciences*, 43(18):10619–10636, 2020.

[15] Ann Mary Joyson and S. Lakshminarayana. Fuzzy graph representation of eye diseases with symptoms and its domination number. In *2nd International Conference on Recent Trends in Applied and Computational Mathematics: ICRTACM-2021*, volume 2649, page 030010. AIP Publishing LLC, 2023.

[16] Hannah B. Gafen, Chin-Chi Liu, Nikole E. Ineck, Clare M. Scully, Melanie A. Mironovich, Christopher M. Taylor, Meng Luo, Marina L. Leis, Erin M. Scott, Renee T. Carter, et al. Alterations to the bovine bacterial ocular surface microbiome in the context of infectious bovine keratoconjunctivitis. *Animal Microbiome*, 5(1):60, 2023.

[17] Kottakkaran Sooppy Nisar, Aqeel Ahmad, Muhammad Farman, Evren Hincal, and Anum Zehra. Modeling and mathematical analysis of fractional order eye infection (conjunctivitis) virus model with treatment impact: Prelicence and dynamical transmission. *Alexandria Engineering Journal*, 107:33–46, 2024.

[18] Mdi Begum Jeelani and Nadiyah Hussain Alharthi. On a symmetry-based structural deterministic fractal fractional order mathematical model to investigate conjunctivitis adenovirus disease. *Symmetry*, 16(10):1284, 2024.

[19] Aqeel Ahmad, Muhammad Owais Kulachi, Ayman A. Aly, Mustafa Inc, M. O. Ahmad, and Shahram Rezapour. Flip bifurcation analysis and investigation of conjunctivitis virus by using sustainable control approach. *Biomedical Signal Processing and Control*, 100:106956, 2025.

[20] Jufren Zakayo Ndendya and Yustina Amon Liana. A deterministic mathematical model for conjunctivitis incorporating public health education as a control measure. *Modeling Earth Systems and Environment*, 11(3):1–17, 2025.

[21] Odo Diekmann, Johan Andre Peter Heesterbeek, and Michael G. Roberts. The construction of next-generation matrices for compartmental epidemic models. *Journal*

of the Royal Society Interface, 7(47):873–885, 2010.

[22] Pauline Van den Driessche and James Watmough. Reproduction numbers and subthreshold endemic equilibria for compartmental models of disease transmission. *Mathematical Biosciences*, 180(1-2):29–48, 2002.

[23] Wendell H. Fleming and Raymond W. Rishel. *Deterministic and Stochastic Optimal Control*, volume 1. Springer Science & Business Media, 2012.

[24] Suzanne Lenhart and John T. Workman. *Optimal Control Applied to Biological Models*. Chapman and Hall/CRC, 2007.

[25] S. I. Oke, M. B. Matadi, and S. S. Xulu. Cost-effectiveness analysis of optimal control strategies for breast cancer treatment with ketogenic diet. *Far East Journal of Mathematical Sciences*, 109(2):303–342, 2018.